Advanced pediatric neuroimaging

Arastoo Vossough[1] ![ORCID]

Abstract

Advanced magnetic resonance neuroimaging techniques play an important adjunct role to conventional MRI sequences for better depiction and characterization of a variety of brain disorders. In this article we briefly review the basic principles and clinical utility of a select number of these techniques, including clinical functional MRI for presurgical planning, clinical diffusion tensor imaging and related techniques, dynamic susceptibility contrast perfusion imaging using gadolinium injection, and arterial spin labeling perfusion imaging. The article focuses on general principles of clinical MRI acquisition protocols, relevant factors affecting image quality, and a general framework for obtaining images for each of these techniques. We also present relevant advances for acquiring these types of imaging sequences in a clinical setting.

Keywords Arterial spin labeling · Brain · Children · Diffusion tensor imaging · Functional magnetic resonance imaging · Magnetic resonance imaging · Perfusion imaging

Introduction

Conventional MRI provides excellent morphologic and anatomical imaging of a variety of brain abnormalities in children and adults alike. These sequences rightfully remain the workhorse tools in the imaging evaluation of primary and secondary brain disorders. Several advanced MRI techniques have become more widespread in recent years as a result of higher-field-strength MRI systems, improved gradients and more widespread availability of relevant acquisition and analysis methods. In this article we focus on a select number of these techniques including functional MRI, diffusion tensor imaging, dynamic susceptibility contrast perfusion imaging and arterial spin labeling perfusion imaging. For each of these techniques, we first briefly review the basic principles and general clinical utility of these techniques, and then focus on general principles of acquisition protocols and recent advances in obtaining these types of imaging sequences.

✉ Arastoo Vossough
    vossough@chop.edu

1   Department of Radiology, Children's Hospital
    of Philadelphia, 3401 Civic Center Blvd., Philadelphia,
    PA 19104, USA

Functional magnetic resonance imaging

Functional MRI (fMRI) utilizing blood oxygenation level–dependent (BOLD) changes has revolutionized the assessment of the brain activity in various fields in the neurosciences. The main utility of fMRI in the clinical environment is for presurgical planning before resection of lesions such as brain tumors, vascular malformations or epileptogenic foci near eloquent cortex. The most commonly interrogated eloquent areas of the brain include motor areas, language areas and visual areas.

The basis for the BOLD response lies in the fact that local neuronal activity is shortly followed by a transient, but more prolonged, focal vasodilatory hemodynamic response, which in turn changes the MRI signal in blood. Deoxyhemoglobin has a higher susceptibility effect than oxyhemoglobin. The focal vasodilatory hemodynamic response causes a relative increase in oxyhemoglobin and a relative decrease in deoxyhemoglobin, and this difference can be detected by targeted MRI sequences. This transient BOLD response change in deoxyhemoglobin/oxyhemoglobin ratio can be characterized as a hemodynamic response function and lasts approximately 3–5 s, much longer than neuronal activity. Performance of clinical fMRI is typically done via various task-based fMRI paradigms while image acquisition is being performed, with subsequent analysis to visualize corresponding regions of brain activation, and finally co-registered to an anatomical

image for display or use in a surgical navigation guidance system. In sedated children, some centers have reported implementing passive limb movement or passive listening with relative success for assessment of the sensorimotor or language regions, respectively [1, 2]. Several preprocessing steps are involved before formal statistical analysis is performed in order to decrease artifacts and allow more robust activation detection. Pixelwise statistical comparison is finally performed between rest and activation periods utilizing varying statistical thresholds to depict areas of activation based on knowledge of functional neuroanatomy.

Functional MRI tasks do not elicit an adequate BOLD response in all situations, for example in the vicinity of arteriovenous malformations and certain brain tumors. This is typically a result of the inability to launch the necessary vasodilatory response. For example, in some cases of arteriovenous malformations, there is already maximum or near-maximum local vasodilation at baseline. In some brain tumor cases, the presence of the tumor with abnormal vasculature hinders mounting of a BOLD response. The phenomenon in which neuronal activity is not coupled to a detectable vascular response is termed neurovascular uncoupling. Cerebral vascular steal phenomena might also contribute to neurovascular uncoupling. In some of these pathological states, a false-negative fMRI does not show the BOLD response and, as such, it could hinder adequate interpretation of fMRI and confound surgical planning. The most important factor for interpretation is awareness of this phenomenon. One way to try to demonstrate this confounder is to perform cerebrovascular reactivity testing of the brain using BOLD. The most common way to perform this is to induce an increased carbon dioxide (CO_2) state, which would result in cerebral vasodilation, and compare the BOLD phenomena at baseline

and after the induced vasodilated state. If an area of the brain shows an impaired BOLD response during cerebrovascular reactivity testing, then one can suspect neurovascular uncoupling in that area of the brain and therefore fMRI interpretation should be made with caution. Induction of a CO_2-related vasodilatory state can be made by breath-holding or, alternatively, by a controlled gas exchange device that can provide a quantitative and standardized stimulus with better reproducibility [3, 4]. However, these devices are unavailable at many institutions or are not approved by the United States Food and Drug Administration (FDA). Implementation of breath-hold cerebrovascular reactivity testing can be more difficult in pediatric age groups compared to adults.

From a clinical MRI acquisition standpoint, typically a gradient echo echoplanar sequence is used to assess the BOLD response. This type of sequence provides sensitivity to susceptibility changes while also being fast enough to capture the temporal changes in the hemodynamic response function and allow adequate spatial coverage. In routine clinical fMRI, a typical time to repetition (TR) is approximately 2,000–3,000 ms. A task-based block design for clinical use typically spans 3–5 min with intermittent task and rest periods of approximately 20–30 s each. Slice thickness is 3–5 mm with a typical matrix size of 64×64. Parallel imaging is often employed, which also has the benefit of slightly decreasing geometric distortion. Use of higher field imaging provides greater sensitivity to BOLD activation.

More recently, MRI acquisition methods have been devised that can accelerate echoplanar readout sequences such as those in fMRI acquisitions. The most important of these is the multiband-simultaneous multi-slice technique using controlled aliasing, which excites and acquires multiple slices during each readout period [5] (Fig. 1). It
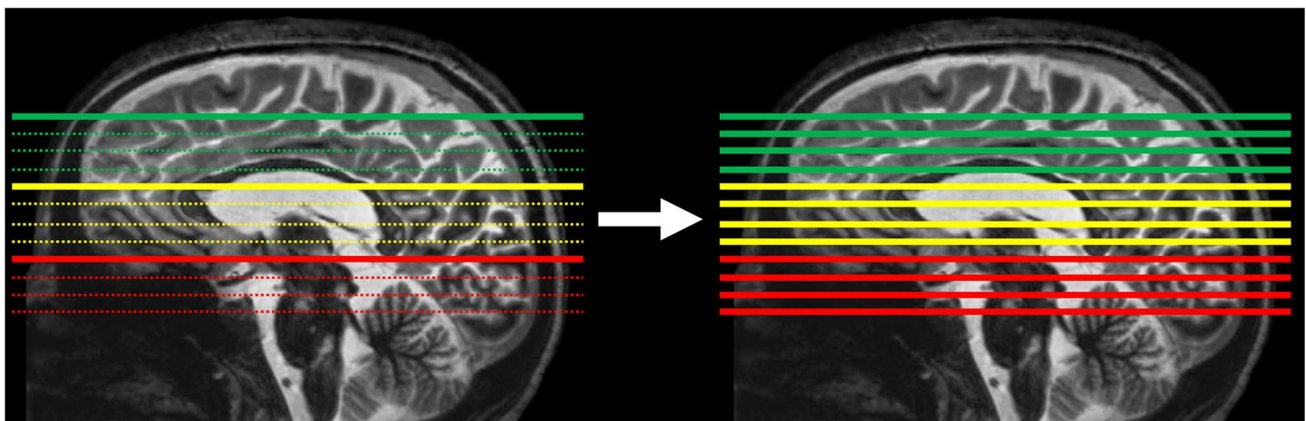

Fig. 1 Multiband simultaneous multi-slice acquisition scheme diagrammed on midline sagittal brain MR images. Compared to regular sequential k-space acquisition, in simultaneous multi-slice there is simultaneous acquisition of multiple k-space lines (*green, yellow, red*) until all lines of k-space are filled. In this particular example, there is a 3-fold acceleration in acquiring k-space. This acquisition scheme results in complex aliasing of the images. Sophisticated methods for removing aliasing allow simultaneous multi-slice to be an effective acceleration method

allows the simultaneous acquisition of different slices with significantly reduced TR, but without significant aliasing, image distortion or large signal-to-noise (SNR) penalty. The advantages of simultaneous multi-slice acquisition in fMRI include higher spatial resolution, greater brain coverage and better temporal resolution for increased sampling rate of the hemodynamic response function (HRF) for higher sensitivity to BOLD changes [6]. For example, if in a 5-min fMRI acquisition with TR=3,000 ms, the hemodynamic response function can be measured 100 times, in an acquisition with 4× simultaneous multi-slice acceleration, the TR can be reduced to 500 ms and therefore HRF can be sampled 400 times in the same 5 min, allowing for more accurate delineation of the HRF curve and potentially better sensitivity and accuracy in depicting BOLD response changes on fMRI (Fig. 2). Of course, the use of simultaneous multi-slice acquisition does not significantly affect the underlying mechanisms involved in neurovascular uncoupling. It remains to be seen whether simultaneous multi-slice (SMS)-enabled presurgical planning fMRI acquisitions will result in better patient surgical outcomes.

Diffusion tensor imaging

Diffusion tensor imaging (DTI) is a type of diffusion imaging that — in addition to measuring diffusivity — by virtue of being acquired in numerous directions can resolve directionality of diffusion changes and therefore quantitate anisotropic diffusion in various directions. This feature allows for the analysis of DTI data in construction of voxelwise fractional anisotropy maps. Additionally, using a variety of deterministic and probabilistic methods, one can depict the direction of tracts (usually white matter tracts) in the brain [7]. This method of analysis and visualization of DTI data is known as diffusion tensor tractography. DTI can depict tissue microstructural changes in the brain, particularly in the white matter, including changes caused by myelination and brain development, the effect of various disorders on brain microstructure, and post-treatment changes. In addition to basic neuroscience evaluation of normal brains, these methods have been applied to a variety of disease categories including developmental, neoplastic, demyelinating and inflammatory disorders. Direction-encoded color maps of fractional anisotropy have been used in clinical delineation of congenital malformations.

Diffusion tractography is used in presurgical mapping of major white matter bundles in select disorders, and various quantitative indices of tract bundles have been investigated in various diseases. A bare minimum number of diffusion gradient directions for DTI is 6, but common acquisition schemes include 12, 20, 30, 42 and 64 direction acquisitions, with increased acquisition time needed as the number of directions rises. Typical clinical DTI is done with a matrix of 128×128 (or slightly higher or lower), and isotropic or near-isotropic voxels would be preferable if tractography were
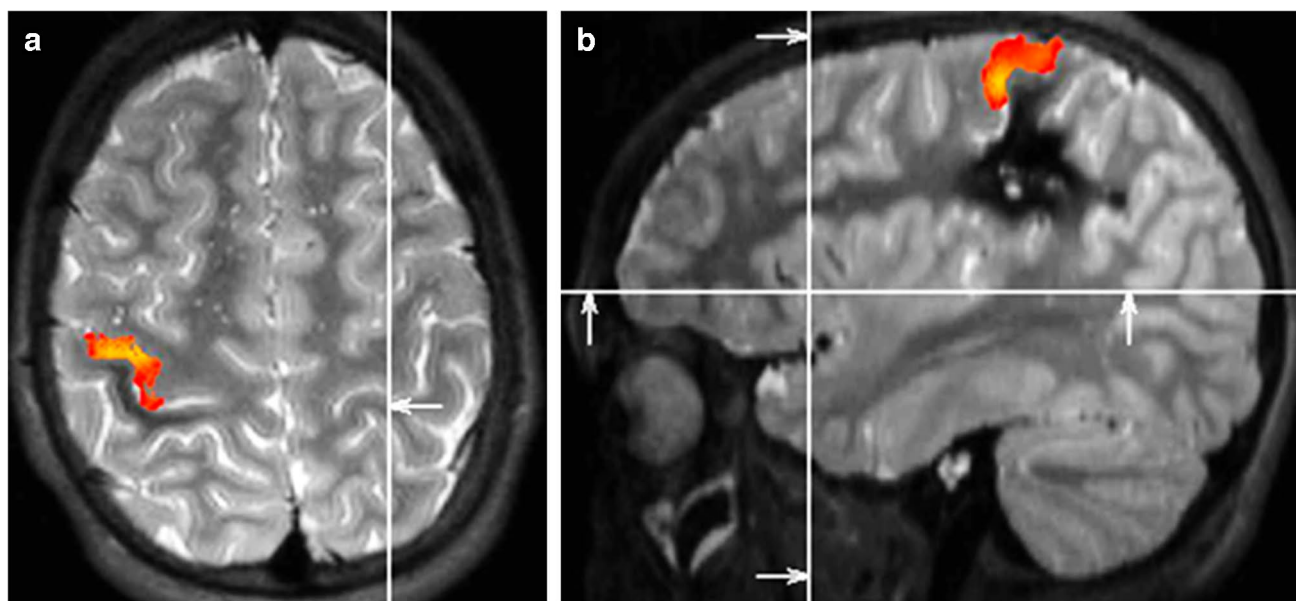

Fig. 2 Presurgical mapping of the hand motor area in a 14-year-old boy with a cavernous malformation. **a, b** Paired axial (**a**) and sagittal (**b**) functional MR images in an anatomical coordinate system (*lines* and corresponding *arrows*). Lower time to relaxation (TR) enabled by simultaneous multi-slice acceleration enables more frequent sampling of the hemodynamic response function and consequently exquisite mapping of the motor activity adjacent to the cavernous malformation, with the activation blob very closely following the gyral anatomy of the precentral gyrus

to be performed on the DTI data. Slice thickness typically ranges between 2 mm and 4 mm. Routine clinical diffusion uses a b value of 1,000 s/mm^2, although in neonates and young infants, lower b values of 600–800 s/mm^2 have been used given the higher water content of the brain in these age groups [8]. High b values (much greater than 1,000 s/mm^2) provide better diffusion sensitivity, particularly for tractography, but they come at a cost of decreased SNR. The time to echo (TE) should be kept to the minimum allowed by the system to increase SNR (less signal loss incurred by T2 relaxation) and to minimize susceptibility and geometric distortion artifacts. Higher field scanners and high-performance gradients enable faster scans and shorter TEs for diffusion imaging. Superconducting closed-bore whole-body scanners typically have gradient slew rates of 30–80 mT/m. Use of new "connectome" scanners in the research setting provides slew rates of 300 mT/m, allowing exquisite diffusion imaging of brain microstructure and anatomical connectivity.

Major limitations of routine diffusion tensor imaging are that it cannot resolve areas containing crossing fibers coursing in different directions within a single voxel, and it cannot track fibers at sharp turns with steep angles. For example, at the junction of major white matter fiber tracts, DTI cannot resolve those tracts. Even in routine tractography of the corticospinal tract, the lower-extremity tracts extending to the corresponding homunculus can be easily resolved given their relatively straight course, whereas tracts in parts the upper extremity and face region are not easily resolved by DTI, given the angular turn in the corticospinal tract fibers corresponding to these areas (Fig. 3). As such, use of DTI in presurgical mapping of these areas of the brain can be limited. A few more advanced diffusion acquisition and analysis techniques (DTI+) can overcome these limitations, including high angular resolution diffusion imaging (HARDI) and diffusion spectrum imaging (DSI). However, these techniques typically use much higher diffusion directions or multiple shells that take a very long time to acquire and therefore are often clinically prohibitive, particularly in the pediatric setting where motion or prolonged sedation becomes problematic in long MRI acquisitions. As such, there is a need for further acquisition acceleration if these types of diffusion analyses are to be employed in patient care settings. Additionally, some of these techniques use b values much higher than 1,000 s/mm^2, with resultant low SNR that would in turn require more advanced scanner hardware for clinical feasibility.

Diffusion images are acquired as spin-echo echoplanar images. Similar to the described fMRI acceleration schemes, multiband-simultaneous multi-slice can be effectively used to accelerate diffusion acquisitions [9]. The advantages of the use of simultaneous multi-slice acquisition in DTI include higher spatial resolution, faster acquisition of typically long advanced diffusion sequences, and the capability
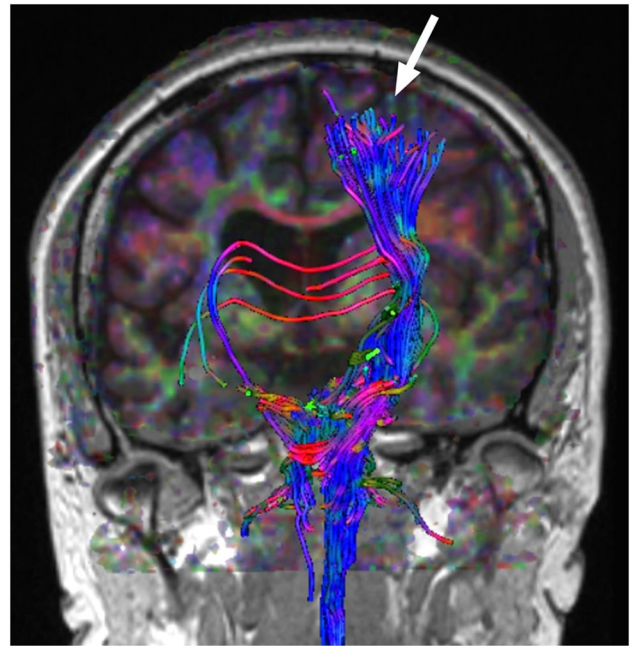

Fig. 3 Diffusion tensor imaging and tractography. Coronal diffusion tensor imaging and tractography along the corticospinal tracts superimposed on T1-weighted MR image demonstrates severely diminished right corticospinal tract compared to the left side in a 7-year-old boy with chronic right-side ischemic brain damage and left hemiplegia. Note that even on the normal side (*arrow*), the tractography depicts the lower-extremity tracts and not the face tracts, given the angulation along those fibers

of improved diffusion resolution with more directions and more b values [10]. Hardware advances and use of simultaneous multi-slice enable acquisition of the more advanced diffusion schemes closer to clinically acceptable timeframes. These accelerated sequences can enable better delineation of tracts in both healthy and presurgical patients [11] and these advanced diffusion methods are expected to become more routine in clinical practice as post-processing and analysis methods become more streamlined.

Dynamic susceptibility contrast perfusion imaging

One of the multiple methods of assessing perfusion in the brain is dynamic susceptibility contrast (DSC) MR imaging. It most commonly uses T2* images over the course of 1–2 min, when a rapid injection of gadolinium-based contrast agent passes through the brain. The gadolinium in high concentration causes changes in susceptibility effects, the signal of which can be transformed into a change in relaxation rate proportional to the fraction of blood volume within each imaging voxel [12, 13]. A large variety of perfusional hemodynamic parameters can be derived from subsequent

analysis of the relaxation time curves from DSC perfusion. The most commonly utilized measures clinically are cerebral blood volume (CBV), cerebral blood flow (CBF), mean transit time (MTT) and time to maximum (T_{max}). Derivation of these hemodynamic parameters requires elaborate post-processing computations that vary by the specific software and processing algorithms.

Although much more commonly performed in adult neuroimaging, assessment of these hemodynamic parameters provides important information in acute and chronic cerebrovascular disease and stroke, initial assessment of brain masses and tumors, and follow-up imaging of a number of cerebral neoplasms after treatment in order to differentiate recurrent tumor from treatment-related changes (Fig. 4) [14–17]. DSC perfusion has also been used in children, again predominantly in preoperative assessment of brain tumor grading and cerebrovascular disease [18, 19].

The appearance and reliability of DSC perfusion imaging maps depend on a number of technical image acquisition and post-processing factors. As far as image acquisition, the main parameters include overall type of acquisition (gradient echo versus spin echo), TR, TE, flip angle, injection bolus, acquisition of one or few pre-injection volumes, number and span of time points acquired, and the presence or absence of a pre-bolus injection of gadolinium contrast material. In order to provide adequate fast temporal resolution during dynamic contrast administration, an echoplanar imaging (EPI)-based acquisition is typically used. Non-standardized and variable DSC acquisition schemes and post-processing

methods have long plagued accuracy and reproducibility of DSC-derived measures and potentially hindered their reliable use in clinical trials. A major confounding factor in DSC perfusion imaging, particularly in the context of brain tumors, is the issue of contrast leakage, which can lead to inaccuracy and underestimation of rCBV in brain tumors. This is primarily caused by T1 contamination as a result of contrast leakage from abnormal and leaky blood–brain barrier in some brain neoplasms. Several post-processing correction algorithms are available to correct and compensate for contrast leakage in these circumstances. It has long been shown that leakage-corrected rCBV maps correlate with tumor grading of gliomas while uncorrected maps do not [20] (Fig. 4).

Recently, expert consensus recommendations were produced after systematic evaluation of various DSC perfusion acquisition and contrast injection schemes [21–24]. Researchers have shown that a gradient echo acquisition with an intermediate (60°) flip angle with field-strength-dependent echo time (TE = 40–50 ms at 1.5 tesla [T]; TE = 20–35 ms at 3 T), along with both a full-dose preload and a full-dose bolus, results in the best accuracy and precision for estimating cerebral blood volume; however, this necessitates a double dose of gadolinium contrast agent, which is less desirable in the era of gadolinium deposition discussions. Alternatively, a no-preload with full-dose contrast agent using a low (30°) flip angle and same field-strength-dependent echo time also provides excellent performance (Table 1) [22, 24]. The latter strategy, in addition to eliminating the
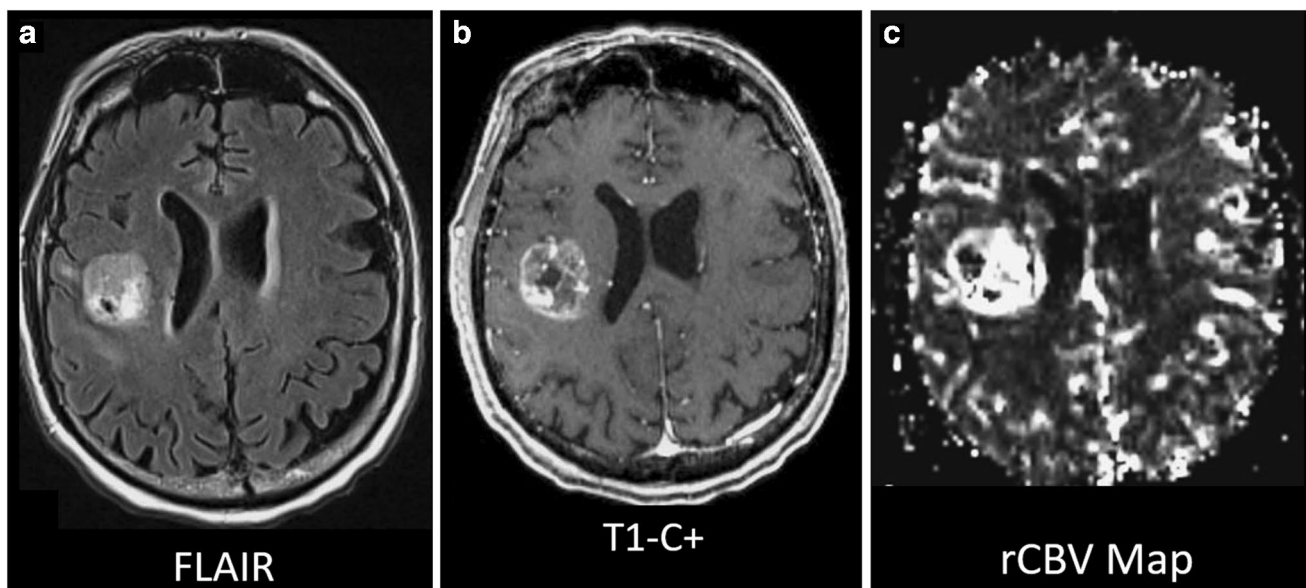

Fig. 4 Dynamic susceptibility contrast perfusion MRI in a brain mass. **a** Axial fluid-attenuated inversion recovery (FLAIR) image shows a hyperintense mass in the right cerebral hemisphere. **b** Axial post-contrast T1-weighted image shows irregular contrast enhancement of the mass. **c** The mass shows elevated relative cerebral blood volume (rCBV) on axial map. This was proved to be a high-grade glioma, as predicted

Table 1 Recommendations for acquisition of dynamic susceptibility contrast perfusion MRI[a]

Acquisition: gradient echo echoplanar imaging		≥120 timepoints acquisition[b]		3–4-mm slice thickness	
	Field strength	Preload dose	Bolus dose	Flip angle	Time to echo (TE)
Best accuracy and precision for CBV	1.5 T	Full	Full	60°	40–50 ms
	3 T	Full	Full	60°	20–35 ms
Also very good performance	1.5 T	None	Full	30°	40–50 ms
	3 T	None	Full	30°	20–35 ms

CBV cerebral blood volume, *T* tesla

[a]Information derived from [22, 24]. Note that these recommendations have not been specifically evaluated in children of various ages

[b]All imaging will have leakage correction in post-processing

need for a double dose of gadolinium contrast agent, could also decrease variation in preload contrast dosing and in incubation times between the preload injection and the actual bolus contrast injection.

Arterial spin labeling imaging

Arterial spin labeling (ASL) perfusion MRI is a perfusion method that does not require exogenous gadolinium tracer administration but rather uses the water in blood as an endogenous tracer. In ASL neuroimaging, brain signal is measured twice, once at baseline and once after tagging (labeling) of arterial blood by inverting the magnetization of water in a slab of tissue. A subtraction image of these two acquisitions results in an image that is proportional to cerebral blood flow. After further post-processing and calculations, quantitative cerebral blood flow maps can be derived. Given that ASL is a subtraction image of two source images, it is quite sensitive to motion. The obvious advantage of ASL compared to DSC perfusion is its non-invasive nature and the lack of need for exogenous intravenous contrast administration (i.e. gadolinium). Other advantages of ASL include easier quantification of flow and the ability to immediately repeat the sequence in cases of motion, poor positioning or artifacts. On the other hand, ASL acquisition times are typically longer than DSC perfusion and there is significantly lower signal-to-noise on ASL images.

Arterial spin labeling has been applied to a variety of neurologic disorders in both adults and children, and various hypoperfusion and hyperperfusion patterns have been defined [25–29]. ASL can depict perfusional changes resulting from various cerebrovascular disorders and anomalies. Seizures, complicated migraines, inflammatory disorders, brain neoplasms and certain neurodegenerative disorders have altered cerebral perfusion and are detectable by ASL perfusion imaging. In a meta-analysis of multiple small studies, ASL was shown to have moderate to good sensitivity and specificity in preoperative differentiation of pediatric high-grade and low-grade tumors [30]. ASL was also shown to be useful in distinguishing pilocytic from pilomyxoid astrocytomas (Fig. 5) [31].

Arterial spin labeling can be acquired using a variety of echoplanar and non-echoplanar sequences. The ways in which ASL sequences can be obtained preclude a strict protocol prescription, but general guidelines can be provided for various aspects of ASL imaging in the clinical setting. The two most common categories of ASL implementation clinically include pulsed arterial spin labeling (PASL) and pseudo-continuous arterial spin labeling (pCASL). Even within these two broad categories, many potential variations exist in terms of labeling schemes and acquisition details. The main advantages and disadvantages of each of these two ASL types are presented in Table 2. Overall, pseudo-continuous ASL is preferred in most circumstances if available on the MRI scanner [32]. A variety of spin-echo echoplanar, 3-D gradient and spin-echo (GRASE), and non-cartesian spiral acquisitions are available from different vendors for ASL acquisition in patients. Because ASL is typically a low SNR technique, imaging voxels are typically larger, with a common imaging matrix being 64×64. Background suppression techniques also help increase the SNR and conspicuity of findings.

Tailoring the ASL acquisition by determining the post-label delay time interval is crucial. This period is the time between the labeling of the blood and acquiring the target images. It can significantly affect the appearance and quality of ASL images (Fig. 6). In a sample of normal children 7–17 years old, the mean arterial transit time on ASL was measured to be 1,538±123 ms [33]. This can serve as a basis for determining appropriate post-label delay times in acquisition of ASL sequences. Post-label delay times between 1,500 ms and 2,100 ms would work well in most children. In a white paper primarily focused on adults, researchers suggested a post-label delay of 1,500 ms in children and

Fig. 5 Arterial spin labeling (ASL) perfusion in two 5-year-old boys with suprasellar astrocytomas. **a, b** First boy. Axial post-contrast T1-weighted MR image (**a**) shows a contrast-enhancing mass, which demonstrates elevated cerebral blood flow (*arrow*) on ASL perfusion imaging (**b**), shown to be a pilomyxoid astrocytoma. **c, d** Second boy. Axial post-contrast T1-weighted MR image (**c**) shows a contrast-enhancing mass without cerebral blood flow elevation (*arrow*) on ASL perfusion imaging (**d**), shown to be a pilocytic astrocytoma
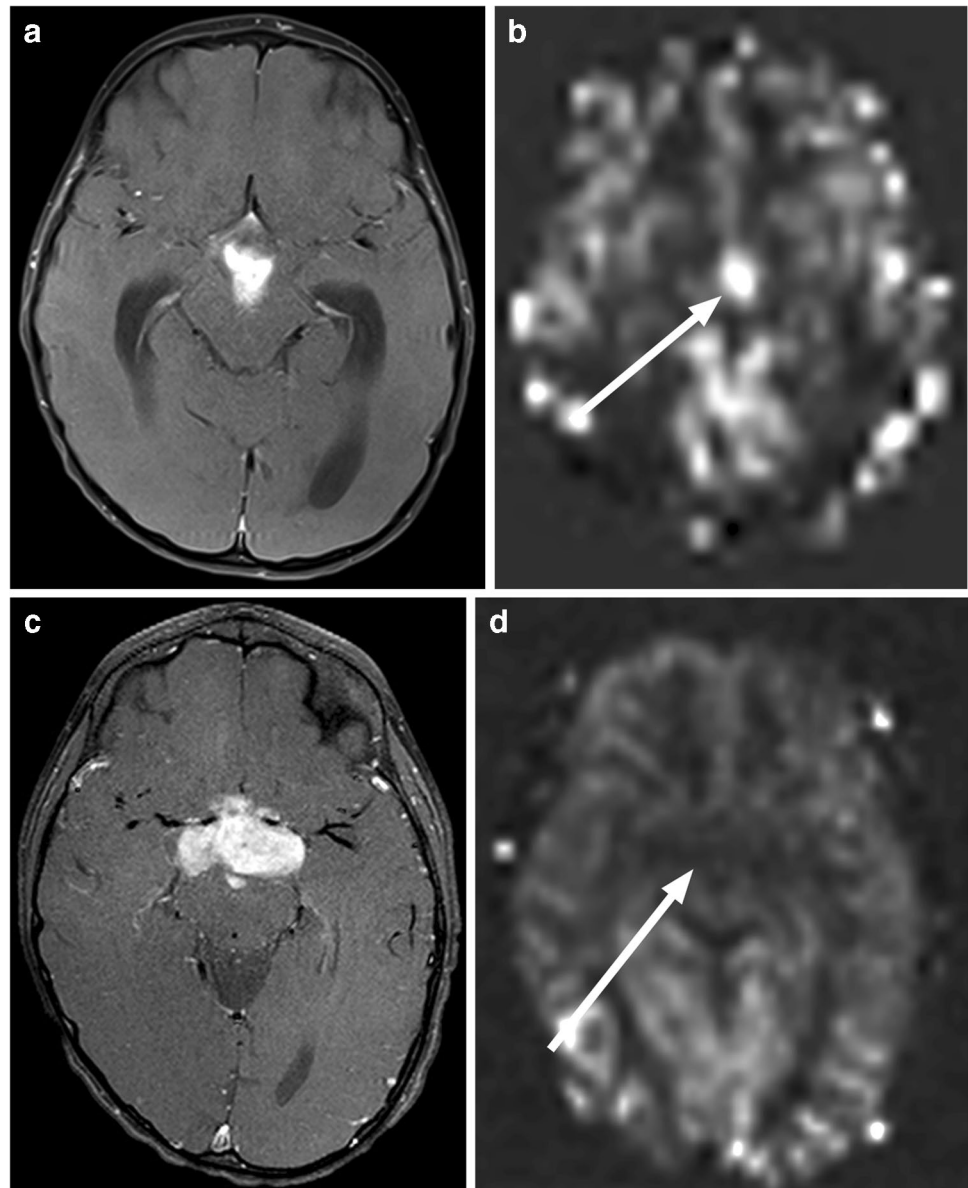

Table 2 Advantages and disadvantages of the two most widely used arterial spin labeling (ASL) categories

Type of ASL	Advantages	Disadvantages
Pulsed ASL (PASL)	Higher tagging efficiency	Lower SNR
Pseudo-continuous ASL (pCASL)	Higher SNR	Lower tagging efficiency
	Less sensitive to tag dispersion	Higher SAR
		More sensitive to B0 and B1 inhomogeneities

SAR specific absorption rate, *SNR* signal-to-noise ratio

2,000 ms in neonates [32], although various vendors have implemented different default post-label delay times. A post-label delay time that is too short results in the label (tag) being within large intracranial arteries at the time of scanning. A post-label delay that is too long results in

disappearance of the label as its signal returns to baseline as a function of longitudinal relaxation. Use of higher magnetic field scanners can slightly prolong the relaxation time of the label, but only marginally. More recently, ASL has been performed with different labeling delay times during
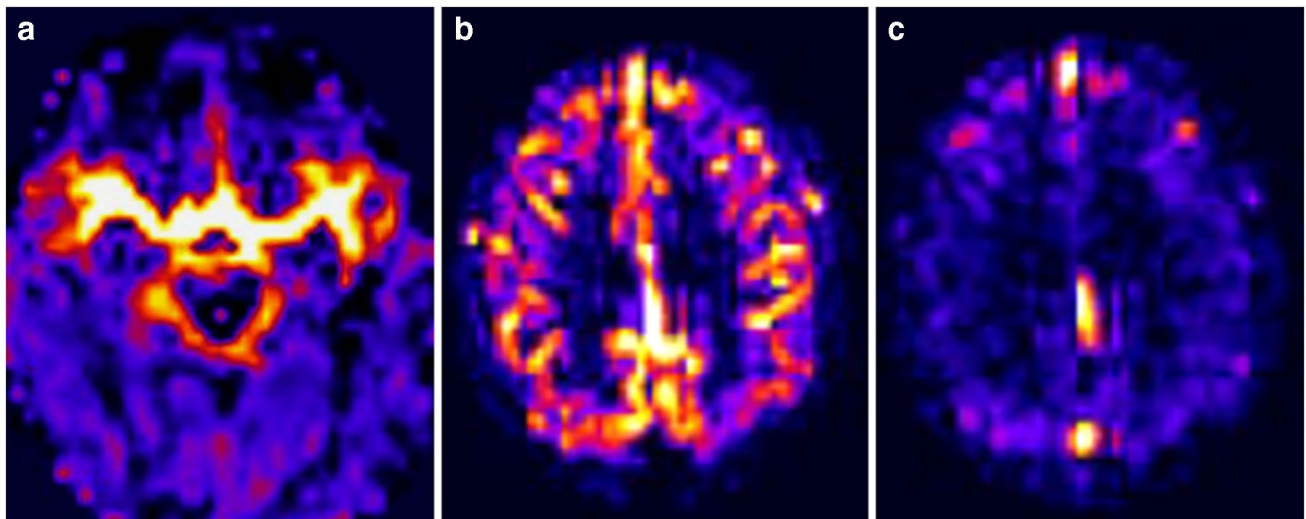
Fig. 6 Effect of post-label delay times on arterial spin labeling (ASL) imaging (all axial images). **a** A post-label delay time that is too short results in the label (tag) remaining within large intracranial arteries at the time of scanning. **b** An appropriate post-label delay demonstrates brain parenchymal perfusion. **c** A post-label delay that is too long results in disappearance of the label as its signal returns to baseline as a function of longitudinal relaxation. This should not be confused with hypoperfusion

an acquisition (multiphase ASL) [34]. This allows depiction and calculation of transit time effects. However, these sequences typically take longer and are not available commercially from all vendors.

One major limitation for conventional ASL sequences, which apply magnetic labels based on the location of arterial spins, is the fact that in cases of arterial transit delay from any cause, the transit delay might exceed the relaxation time of the magnetic label. As such, there is not enough residual label left, hence robust measures of cerebral blood flow cannot be obtained, for example in cases with significant arterial stenosis. One potential solution to this limitation is a relatively newer form of ASL named velocity-selective ASL that does not require spatial selectivity [35]. This technique is relatively insensitive to transit-delay artifacts. Therefore, it can be used to accurately delineate cerebral blood flow in people with such delays, like those with moyamoya disease [36]. However, this technique is not FDA-approved or commercially available and it needs further optimization to decrease artifacts.

Conclusion

Advanced neuroimaging techniques can be important adjuncts to conventional brain MRI. They provide additional information that in select cases could be crucial for diagnosis or surgical planning. A summary of indications and acquisition times is in Table 3. Recent advances in scanner hardware, new and improved sequences, novel acceleration

Table 3 Summary of major clinical indications and typical acquisition times of advanced neuroimaging techniques

Technique	Imaging times	Main clinical indications
Functional MRI (task-based)	3–6 min (per task)	Presurgical mapping of eloquent brain cortical regions
Diffusion tensor imaging	2–15 min	Presurgical planning of white matter tracts
		Adjunct to evaluation of brain malformations
		Adjunct to assessment of brain maturation
Dynamic susceptibility contrast perfusion imaging	1–2 min	Preoperative assessment of brain masses and tumors
		Post-treatment assessment of brain tumors
		Acute and chronic cerebrovascular diseases
Arterial spin-labeling perfusion imaging	2–8 min	Preoperative assessment of brain masses and tumors
		Post-treatment assessment of brain tumors
		Cerebrovascular diseases
		Seizure localization (often peri-ictal)

schemes and better analysis software have gradually enabled incorporation of many of these techniques into the clinical arena. Knowledge of the basic principles behind these sequences and optimization of the associated protocols can further enhance their clinical reliability and clinical integration. It is anticipated that future advances and standardization efforts will increase reliability and more widespread use of these methods.

Declarations

Conflicts of interest None

References

1. Vannest JJ, Karunanayaka PR, Altaye M et al (2009) Comparison of fMRI data from passive listening and active-response story processing tasks in children. J Magn Reson Imaging 29:971–976
2. Ogg RJ, Laningham FH, Clarke D et al (2009) Passive range of motion functional magnetic resonance imaging localizing sensorimotor cortex in sedated children. J Neurosurg Pediatr 4:317–322
3. Pillai JJ, Mikulis DJ (2015) Cerebrovascular reactivity mapping: an evolving standard for clinical functional imaging. AJNR Am J Neuroradiol 36:7–13
4. Fierstra J, Sobczyk O, Battisti-Charbonney A et al (2013) Measuring cerebrovascular reactivity: what stimulus to use? J Physiol 591:5809–5821
5. Setsompop K, Gagoski BA, Polimeni JR et al (2012) Blipped-controlled aliasing in parallel imaging for simultaneous multislice echo planar imaging with reduced g-factor penalty. Magn Reson Med 67:1210–1224
6. Setsompop K, Feinberg DA, Polimeni JR (2016) Rapid brain MRI acquisition techniques at ultra-high fields. NMR Biomed 29:1198–1221
7. Bucci M, Mandelli ML, Berman JI et al (2013) Quantifying diffusion MRI tractography of the corticospinal tract in brain tumors with deterministic and probabilistic methods. Neuroimage Clin 3:361–368
8. Robertson RL, Ben-Sira L, Barnes PD et al (1999) MR line-scan diffusion-weighted imaging of term neonates with perinatal brain ischemia. AJNR Am J Neuroradiol 20:1658–1670
9. Setsompop K, Cohen-Adad J, Gagoski BA et al (2012) Improving diffusion MRI using simultaneous multi-slice echo planar imaging. Neuroimage 63:569–580
10. Feinberg DA, Setsompop K (2013) Ultra-fast MRI of the human brain with simultaneous multi-slice imaging. J Magn Reson 229:90–100
11. Sanvito F, Caverzasi E, Riva M et al (2020) fMRI-targeted high-angular resolution diffusion MR tractography to identify functional language tracts in healthy controls and glioma patients. Front Neurosci 14:225
12. Rosen BR, Belliveau JW, Aronen HJ et al (1991) Susceptibility contrast imaging of cerebral blood volume: human experience. Magn Reson Med 22:293–299
13. Rosen BR, Belliveau JW, Vevea JM, Brady TJ (1990) Perfusion imaging with NMR contrast agents. Magn Reson Med 14:249–265
14. Aronen HJ, Gazit IE, Louis DN et al (1994) Cerebral blood volume maps of gliomas: comparison with tumor grade and histologic findings. Radiology 191:41–51
15. Grandin CB (2003) Assessment of brain perfusion with MRI: methodology and application to acute stroke. Neuroradiology 45:755–766
16. Okuchi S, Rojas-Garcia A, Ulyte A et al (2019) Diagnostic accuracy of dynamic contrast-enhanced perfusion MRI in stratifying gliomas: a systematic review and meta-analysis. Cancer Med 8:5564–5573
17. Patel P, Baradaran H, Delgado D et al (2017) MR perfusion-weighted imaging in the evaluation of high-grade gliomas after treatment: a systematic review and meta-analysis. Neuro Oncol 19:118–127
18. Testud B, Brun G, Varoquaux A et al (2021) Perfusion-weighted techniques in MRI grading of pediatric cerebral tumors: efficiency of dynamic susceptibility contrast and arterial spin labeling. Neuroradiology 63:1353–1366
19. Ibrahim M, Ghazi TU, Bapuraj JR, Srinivasan A (2021) Contrast pediatric brain perfusion: dynamic susceptibility contrast and dynamic contrast-enhanced MR imaging. Magn Reson Imaging Clin N Am 29:515–526
20. Boxerman JL, Schmainda KM, Weisskoff RM (2006) Relative cerebral blood volume maps corrected for contrast agent extravasation significantly correlate with glioma tumor grade, whereas uncorrected maps do not. AJNR Am J Neuroradiol 27:859–867
21. Ellingson BM, Bendszus M, Boxerman J et al (2015) Consensus recommendations for a standardized brain tumor imaging protocol in clinical trials. Neuro Oncol 17:1188–1198
22. Boxerman JL, Quarles CC, Hu LS et al (2020) Consensus recommendations for a dynamic susceptibility contrast MRI protocol for use in high-grade gliomas. Neuro Oncol 22:1262–1275
23. Bell LC, Semmineh N, An H et al (2019) Evaluating multisite rCBV consistency from DSC-MRI imaging protocols and post-processing software across the NCI quantitative imaging network sites using a digital reference object (DRO). Tomography 5:110–117
24. Schmainda KM, Prah MA, Hu LS et al (2019) Moving toward a consensus DSC-MRI protocol: validation of a low-flip angle single-dose option as a reference standard for brain tumors. AJNR Am J Neuroradiol 40:626–633
25. Atlas SW, Howard RS 2nd, Maldjian J et al (1996) Functional magnetic resonance imaging of regional brain activity in patients with intracerebral gliomas: findings and implications for clinical management. Neurosurgery 38:329–338
26. Deibler AR, Pollock JM, Kraft RA et al (2008) Arterial spin-labeling in routine clinical practice, part 1: technique and artifacts. AJNR Am J Neuroradiol 29:1228–1234
27. Deibler AR, Pollock JM, Kraft RA et al (2008) Arterial spin-labeling in routine clinical practice, part 2: hypoperfusion patterns. AJNR Am J Neuroradiol 29:1235–1241
28. Deibler AR, Pollock JM, Kraft RA et al (2008) Arterial spin-labeling in routine clinical practice, part 3: hyperperfusion patterns. AJNR Am J Neuroradiol 29:1428–1435
29. Haller S, Zaharchuk G, Thomas DL et al (2016) Arterial spin labeling perfusion of the brain: emerging clinical applications. Radiology 281:337–356
30. Delgado AF, De Luca F, Hanagandi P et al (2018) Arterial spin-labeling in children with brain tumor: a meta-analysis. AJNR Am J Neuroradiol 39:1536–1542
31. Nabavizadeh SA, Assadsangabi R, Hajmomenian M et al (2015) High accuracy of arterial spin labeling perfusion imaging in differentiation of pilomyxoid from pilocytic astrocytoma. Neuroradiology 57:527–533

32. Alsop DC, Detre JA, Golay X et al (2015) Recommended implementation of arterial spin-labeled perfusion MRI for clinical applications: a consensus of the ISMRM Perfusion Study Group and the European Consortium for ASL in Dementia. Magn Reson Med 73:102–116

33. Jain V, Duda J, Avants B et al (2012) Longitudinal reproducibility and accuracy of pseudo-continuous arterial spin-labeled perfusion MR imaging in typically developing children. Radiology 263:527–536

34. Fazlollahi A, Bourgeat P, Liang X et al (2015) Reproducibility of multiphase pseudo-continuous arterial spin labeling and the effect of post-processing analysis methods. Neuroimage 117:191–201

35. Wong EC, Cronin M, Wu WC et al (2006) Velocity-selective arterial spin labeling. Magn Reson Med 55:1334–1341

36. Bolar DS, Gagoski B, Orbach DB et al (2019) Comparison of CBF measured with combined velocity-selective arterial spin-labeling and pulsed arterial spin-labeling to blood flow patterns assessed by conventional angiography in pediatric moyamoya. AJNR Am J Neuroradiol 40:1842–1849